Measuring Vibrational Modes in Living Human Cells

Verónica Puerto-Belda, Jose J. Ruz ⬤, Carmen Millá, Álvaro Cano, Marina L. Yubero ⬤, Sergio García ⬤,
Priscila M. Kosaka, Montserrat Calleja, and Javier Tamayo ⬤*

Instituto de Micro y Nanotecnología, IMN-CNM, CSIC (CEI UAM+CSIC), 28760 Tres Cantos, Madrid, Spain

The question of whether human living cells in physiological conditions exhibit mechanical resonances has remained unresolved for more than 70 years. We here construct a theoretical model to predict how these hypothetical vibration modes of a living cell can modify the stochastic response of a supporting micromechanical resonator. The key signatures that demonstrate the existence of these vibration modes are then searched for experimentally. To this aim, single human breast epithelial cells were attached to the surface of compliant small microcantilevers. Close examination of the frequency spectra of the thermal fluctuations of the microcantilever over a high-frequency range of 1 kHz–1 MHz revealed anomalies that are consistent with our theoretical predictions. We identify the stochastic coupling of the first and third vibration modes of the cell with the torsional and flexural vibration modes of the cantilever, respectively. These mechanical resonances are very broad and are located at 10–30 kHz and 150–180 kHz, respectively. The analysis of the experiments allows us to obtain information on the temporal evolution of several physical properties of the cell, in addition to the resonance frequencies, during the adhesion process—such as the mass, viscoelasticity, and contact area. These results open multiple avenues in our understanding of single cell mechanobiology, vibrational spectrometry of living cells and mechanical destruction of cancerous cells by targeting specific cell frequencies.

I. INTRODUCTION

The question of whether living cells exhibit mechanical resonances as any solidlike body was raised by Ackerman during the 1950s [1–3]. He studied the interaction of acoustic fields with living cells such as animal erythrocytes and paramecia, finding that cells break down more easily at characteristic frequencies that can be related to mechanical resonances. These works were rapidly forgotten due to the lack of robust experimental evidence. The question was revisited in 2005 by Zinin *et al.*, who developed theoretical models to calculate the vibrational properties of living cells and predict the interaction between ultrasound fields and cells [4,5]. These models predict resonance frequencies associated to the fundamental quadrupole mode of cells free in fluid of about 5 MHz for 1 μm diameter bacteria and of about 160 kHz for 9-μm-diameter *yeast* cells. The expected quality factors (*Q*s) of these resonances are very low, 1–7, due to fluid damping. However, to date, these predictions have not been confirmed experimentally. Very recent experiments using ultrasensitive optomechanical devices have revealed mechanical resonances of single bacterial cells in vacuum and air [6,7]. In these low-dissipation environments, the fluid damping is

low and cells exhibit elasticlike behavior. More importantly, these cells may be dead or in a nonfunctional biological state. Observation of mechanical resonances of living cells requires measurements in a culture medium where the cells are biologically active and they can naturally grow and divide. However, these environments are highly dissipative due to the strong interaction of the fluid with the cell wall [5]. In addition, more complex cells, such as human cells, are highly heterogeneous, comprising solidlike structures (cytoskeleton, organelles, and macromolecules) bathed in an interstitial fluid (cytosol) [8–11]. The mechanical response of the cells is highly dependent on the frequency, varying from elasticlike to viscouslike behavior and evolving from uniform dynamics to more localized dynamics in cell components [12]. Given these factors, it is uncertain whether complex living human cells in physiological conditions can sustain mechanical resonances. However, if these resonances do exist, they could revolutionize our comprehension of single cell mechanobiology, offering intriguing possibilities in cell fingerprinting and the utilization of mechanical vibrations to stimulate cell behavior and selectively eradicate cancerous cells [13]. Indeed, the impact of low-frequency mechanical vibrations, ranging from 1 to 100 Hz, on cell proliferation, stem cell differentiation, cell behavior, and cell fate is beginning to be recognized [14–16].

The aim of this work is to definitively answer the question originally formulated by Ackerman: "Do biological cells exhibit mechanical resonances?" To this aim we attach single living human breast epithelial cells to the surface of small microcantileverlike resonators in physiological conditions. In addition, we develop a theoretical framework to predict the effect of stochastic coupling between the vibration modes of the cell and the microcantilever. We then probe the stochastic
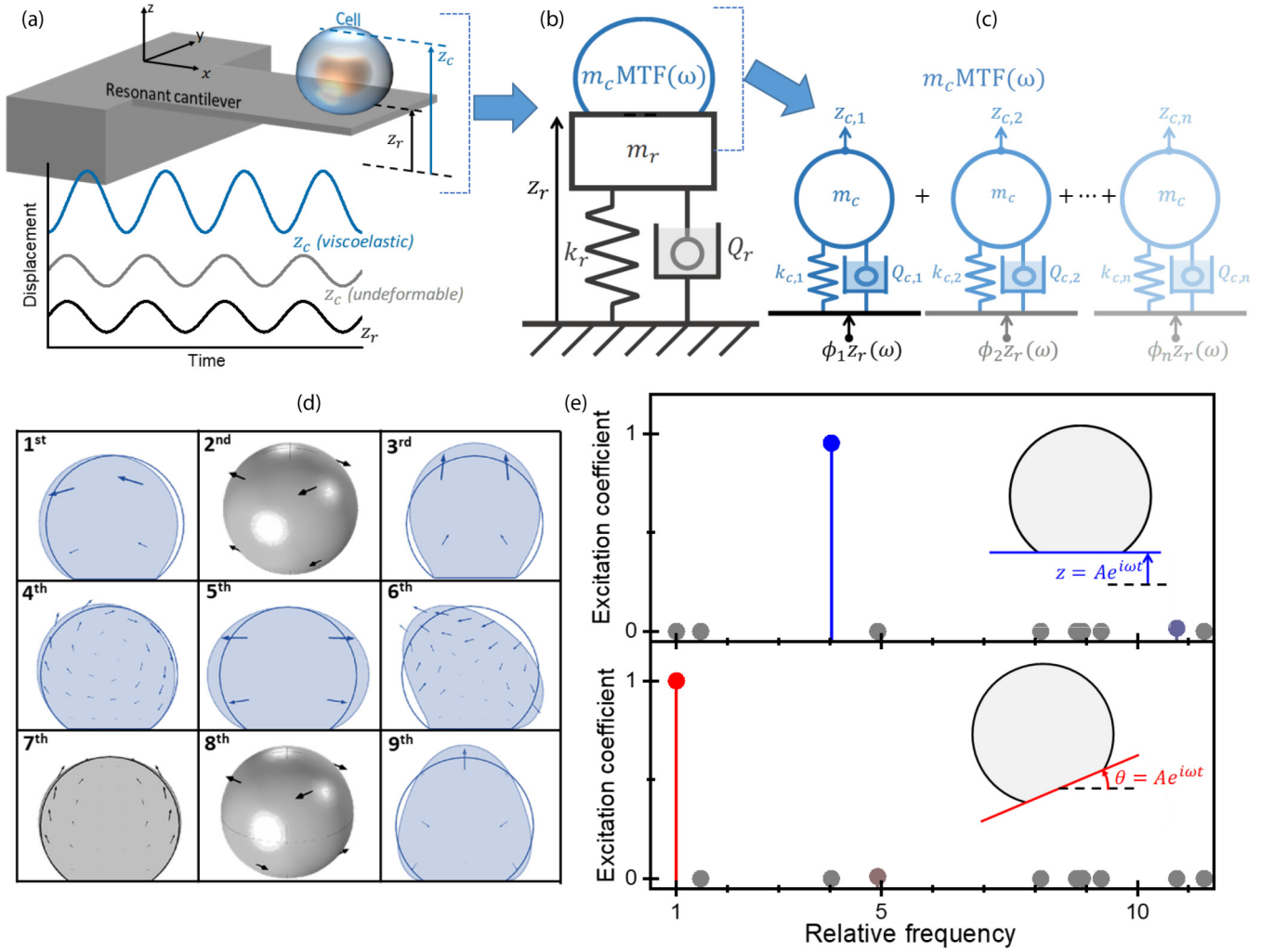
---

*javier.tamayo@csic.es

FIG. 1. Theory of the mechanical interaction between a living cell and a micromechanical resonator. (a) 3D cartoon of a cell on the microcantilever (top). The cantilever oscillation (z_r) is transmitted to the cell (z_c) (bottom). When the cell is infinitely rigid, it oscillates in sync with the cantilever. However, living cells are soft and viscoelastic, which results in a different oscillation amplitude and a phase lag. (b) Schematics of the model of the interaction between a vibration mode of the cantilever and the cell. The cantilever vibration mode is represented as a damped harmonic oscillator loaded by a frequency-dependent complex mass given by the product of the mass of the cell (m_c) and the mass transfer function MTF. (c) Schematic of the mass transfer function of the cell that encloses information on the cell vibration modes and their coupling with the cantilever vibration modes of the cell through the coefficients ϕ_i. (d) Schematic of the first vibration modes of a sphere attached to a surface obtained by FEM. Azimuthal and spheroidal modes are represented in grey and blue tones, respectively. (e) Excitation coefficients (ϕ_n^2) computed by FEM for the cell vibration modes shown in (d) for vertical (top) and tilting oscillation (bottom) of the contact surface. The data show that tilting oscillation efficiently excites the first vibration mode of the cell with negligible contribution of the rest of the modes. Similarly, out-of-plane oscillation efficiently excites the third vibration mode of the cell.

fluctuations of the microcantilever in a wide frequency window between 1 kHz and 1 MHz, searching for the signatures predicted by the theory that reveal the existence of vibration modes of the cell.

II. THEORY

We develop a three-dimensional (3D) theoretical model to predict the effect of a viscoelastic body (the cell) on the vibrational properties of the cantilever; the model is fully detailed in the Supplemental Material (SM) [17]. Within the linear viscoelasticity regime [18], the model demonstrates that the extraordinary complexity of the problem can be reduced

without loss of generality to a damped harmonic oscillator representing a vibration mode of the resonator that is loaded by a frequency-dependent complex mass that can be expressed as the product of the cell mass, m_c, and the mass transfer function, MTF(ω), given by (Figs. 1(a)–1(c); see Sec. I of the SM [17]),

$$\text{MTF} = \sum_{k=1}^{\infty} \phi_k^2 [1 + m_c \omega^2 \chi_k(\omega)], \qquad (1)$$

where $\chi_k(\omega)$ is the mechanical susceptibility of the kth vibration mode of the cell that linearly relates the displacement to the force in the frequency domain, and ϕ_k is the average

projection of the kth eigenmode displacements within the cell on the direction of the cantilever motion,

$$\phi_k = \frac{\int_{V_C} \vec{u_r} \, \vec{\Phi_k} \, dV}{V_C}, \qquad (2)$$

where $\vec{u}_r$ is a unit vector that represents the direction of motion of the cantilever vibration mode at the contact between the cell and the cantilever, $\vec{\Phi_k}$ is the kth cell eigenmode function, and V_C is the cell volume. Since the eigenmode set $\vec{\Phi_k}$ forms an orthonormal basis of the function space of kinematically admissible displacements in the body, the projection coefficients satisfy $\sum_{k=1}^{\infty} \phi_k^2 = 1$. This condition applied to Eq. (1) implies that the mass transfer function is 1 for frequencies much lower than the frequency of the first excitable vibration mode of the cell and zero for frequencies much higher than the last excitable mode of the cell.

The essence of the problem is determining an appropriate description of the mass transfer function of a living cell. This requires two steps: (1) calculation of the vibration modes of the adhered cell and (2) calculation of the coefficients ϕ_k^2, referred to as excitation coefficients, that determine which vibration modes of the cell can be coupled to the cantilever vibration modes. These calculations are performed by combining our theory with finite element method (FEM) simulations.

For the sake of simplicity, we assume that the cell behaves as an isotropic and homogeneous viscoelastic sphere attached to a surface. The viscoelasticity of the cell is described by a complex elastic modulus that obeys a power-law behavior, $E_c(\omega) = E_0(i\frac{\omega}{\omega_0})^{\beta}$, where E_0 is the elasticity modulus at the reference frequency ω_0, and β is the power-law exponent that can range between 0 (elastic solid) and 1 (viscous liquid) [19,20]. In general, the viscoelasticity of the cells is more accurately described by a weak power-law term with $\beta \approx 0.1-0.3$ that dominates for frequencies below approximately 100 Hz and a strong power-law term with $\beta \approx 0.4-0.95$ that becomes dominant for frequencies higher than approximately 1 kHz [12,21]. For the high-frequency range studied here, the first term can be neglected. Figure 1(d) shows the first vibration modes of the cell calculated by the finite element method (FEM). The modes are here split into azimuthal vibration modes and spheroidal modes. The azimuthal vibration modes, which include the second, seventh, and eighth modes, are characterized by tangential motion without any change in volume or the center of mass. On the other hand, the spheroidal modes, which comprise the remaining modes, are characterized by changes in volume, shape, and/or a net displacement of the center of mass. Now, we calculate the excitation coefficients (ϕ_n^2) of the cell vibration modes for two classes of cantilever motion: vertical (z axis) oscillation that is dominant in the flexural vibration modes and tilting oscillation characteristic of torsional vibration modes [Fig. 1(e)]. Azimuthal vibration modes of the cell are not excited by the cantilever vibration modes as expected from examination of Eq. (2). Interestingly, the cell fundamental vibration mode, which is characterized by a net angular displacement of the cell symmetry axis, can be efficiently excited by the torsional vibration of the cantilever. Conversely, the cantilever flexural vibration modes can effectively excite the cell third vibration

mode, which is characterized by an extension or compression deformation of the cell along the vertical direction. The rest of the spheroidal modes are negligibly coupled to the flexural and torsional vibration modes of the cantilever. Hereinafter, the fundamental and third vibration modes of the cell are referred to as the bending and extensional vibration modes of the cell, respectively. Our analysis indicates that these cell vibration modes can be coupled to the torsional and flexural vibrations of a microcantilever, respectively. We now analyze the optimal conditions to observe stochastic coupling between these cell vibration modes and the cantilever vibration modes.

For the sake of convenience, we split the mass transfer function into its real part and the minus imaginary part, i.e., MTF = MTF$'$ − i MTF$''$. The term MTF$'$ modulates the "apparent" cell mass that loads the microcantilever, whereas MTF$''$ increases the dissipation of the microcantilever upon cell attachment. We calculate MTF$'$ and MTF$''$ for power-law exponents β of 0.4, 0.6, and 0.8 [Fig. 2(a)]. In this highly damped system, the resonance frequency of the cell (ω_c) is defined as the frequency where cell dissipation is at its maximum (see Sec. II of the SM [17]). The real part of the mass transfer function exhibits a sigmoidal shape that goes from 1 at $\omega \ll \omega_c$ to 0 at $\omega \gg \omega_c$ passing by $\frac{1}{2}$ at $\omega = \omega_c$. The transition is broader as the dissipation is higher, i.e., as β increases. For $\beta \lesssim 0.6$, MTF$'$ increases above 1 before resonance, making the apparent mass higher than the real mass, and it turns into negative after resonance, resulting in negative apparent masses. The minus imaginary part of the mass transfer function exhibits a Gaussian shape with maximum at resonance. The peak flattens and broadens as the dissipation increases. The impact of the mass transfer function of the cell on the frequency response of a resonator's vibration mode is shown in Fig. 2(b). In these calculations, the resonator quality factor is 3 and the mass ratio between the cell and the cantilever 0.56, similar to our experimental values. For $\beta = 0.4$, the resonance peak splits into two peaks when the resonator frequency is about twice the resonance frequency of the cell. As the resonator frequency increases, the two peaks separate and the amplitude of the first peak decreases. As the cell dissipation increases the peak splitting becomes less visible. For $\beta = 0.6$, a shoulder at the left of the main resonance peak is observed instead of two clear peaks, whereas for $\beta = 0.8$, a peak broadening is only observed. This analysis indicates that the optimal conditions for observing the effect of a cell vibration mode are achieved when the first resonance frequency of the cantilever is moderately higher than the resonance frequency of the first excitable mode of the cell. We now estimate the resonance frequencies of the bending and extensional vibration modes of the cell, which can be expressed as

$$\omega_n = \frac{\lambda_n\left(\frac{a}{R}\right)}{R} \sqrt{\frac{|E_c(\omega_n)|}{\rho_c}}, \qquad (3)$$

where λ_n is a function of the ratio of the contact radius (a) to cell radius (R), and ρ_c is the cell density. The resonance frequencies of the bending and extensional vibration mode of the cell are calculated for a radius of 9 μm as a function of the elasticity modulus for a/R between 0.1 and 0.5 [Fig. 2(c)].
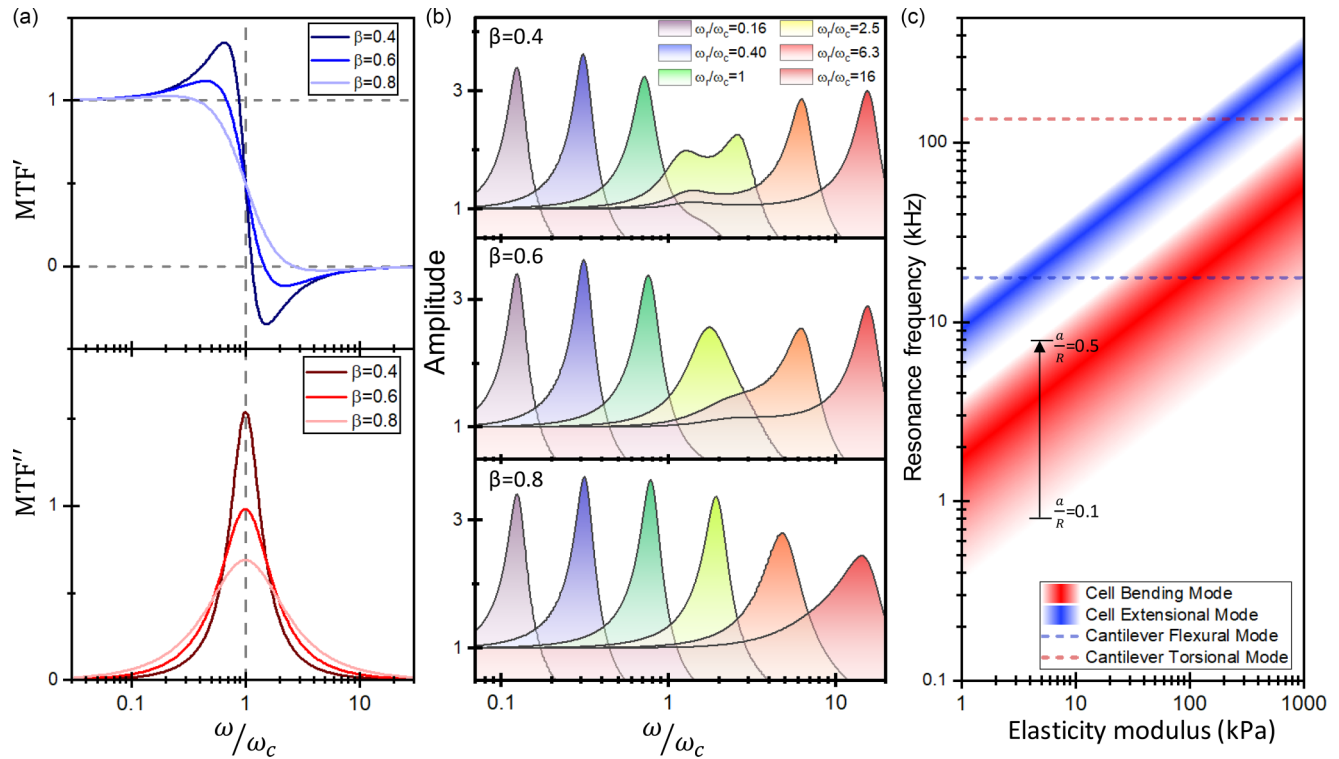
FIG. 2. Effect of the cell mechanical resonances on the frequency spectra of a micromechanical resonator. (a) Theoretical mass transfer function (MTF) for a viscoelastic cell assuming that only a single mode of the cell is excited. The cell's viscoelasticity is described by a complex elastic modulus that follows a power-law behavior. The graphs show the real (MTF′) and the minus imaginary (MTF″) parts of the mass transfer function for power-law exponents β of 0.4, 0.6, and 0.8. (b) Effect of the theoretical mass transfer functions on the resonator frequency response for different ratios between the resonance frequencies of the resonator and the cell (ω_r/ω_c). The quality factor of the resonator is 3 and the cell mass to resonator mass ratio is 0.56, similar to the experiments. (c) Resonance frequencies of the bending and extensional modes of the cell calculated by FEM. The cell radius is 9 μm and the density 1000 kg/m³. The frequency bands arise from varying the radius of the contact area a from 0.1 to 0.5 times the cell radius R. The color intensity peaks at $a/R = 0.25$ and vanishes at 0 and 0.5. The resonance frequencies of the first flexural and torsional vibration modes of the cantilever used in the experiments are plotted as a reference.

Data on the modulus of elasticity of cells at frequencies significantly above 10 kHz are limited, but it is estimated to range from tens to hundreds of kPa. In this range, the frequencies of the bending and extensional vibration modes are approximately located at the frequency windows of 3–30 kHz and 30–300 kHz, respectively. The frequencies of the first flexural and torsional vibration modes of the cantilever used in the experiments are of about 15 and 135 kHz, respectively. In these conditions, weak or negligible coupling is expected between the first flexural mode of the cantilever and the cell extensional mode. However, the resonance frequency of the first torsional mode of the cantilever is well above the expected resonance frequency of the bending mode of the cell. In these conditions, it can be expected the effect of this resonance on the frequency spectra of the cantilever torsional fluctuations.

III. EXPERIMENTAL RESULTS AND MODELING

We describe here the experimental validation of our model with living human breast epithelial MCF-10A cells. The experiments are carried out with an atomic force microscope (AFM) mounted on an inverted optical microscope [Fig. 3(a)]. We use small Au-coated silicon nitride microcantilevers, 50 μm long, 20 μm wide, and 270 nm thick to capture single cells. The microcantilevers are treated with the extracellular matrix protein fibronectin to promote cell adhesion. The microcantilever end is positioned onto the center of the selected cell in the culture dish. It is then brought into contact with the cell maintaining a force of 3 nN for 10 min to ensure cell adhesion [22,23]. Subsequently, the microcantilever is withdrawn with the living cell attached to its surface. The experiments are conducted in a culture medium at 37 °C. Optical microscopy is used to track the position, shape, and size of the cell [Fig. 3(b)]. After attachment, the cell assumes a spherical form and can move around the initial attachment point without exceeding the boundaries of the microcantilever [Figs. 3(b) and 3(c)]. Simultaneously, the cantilever fluctuations are monitored by the laser beam deflection method, allowing for independent measurements of the flexural and torsional motions [24]. Figure 3(d) shows the frequency spectra of the flexural and torsional fluctuations of the cantilever before and after the attachment of a MCF-10A breast epithelial cell. The unloaded cantilever's spectra display three flexural and two torsional vibration modes. Upon cell attachment, notable alterations are observed in the cantilever's flexural and torsional fluctuation frequency spectra. A prominent change is the emergence of a broad shoulder at the left side of the first torsional resonance peak, with its frequency and amplitude increasing over time. This phenomenon aligns with our theoretical predictions [see Fig. 2(b)], indicating stochastic
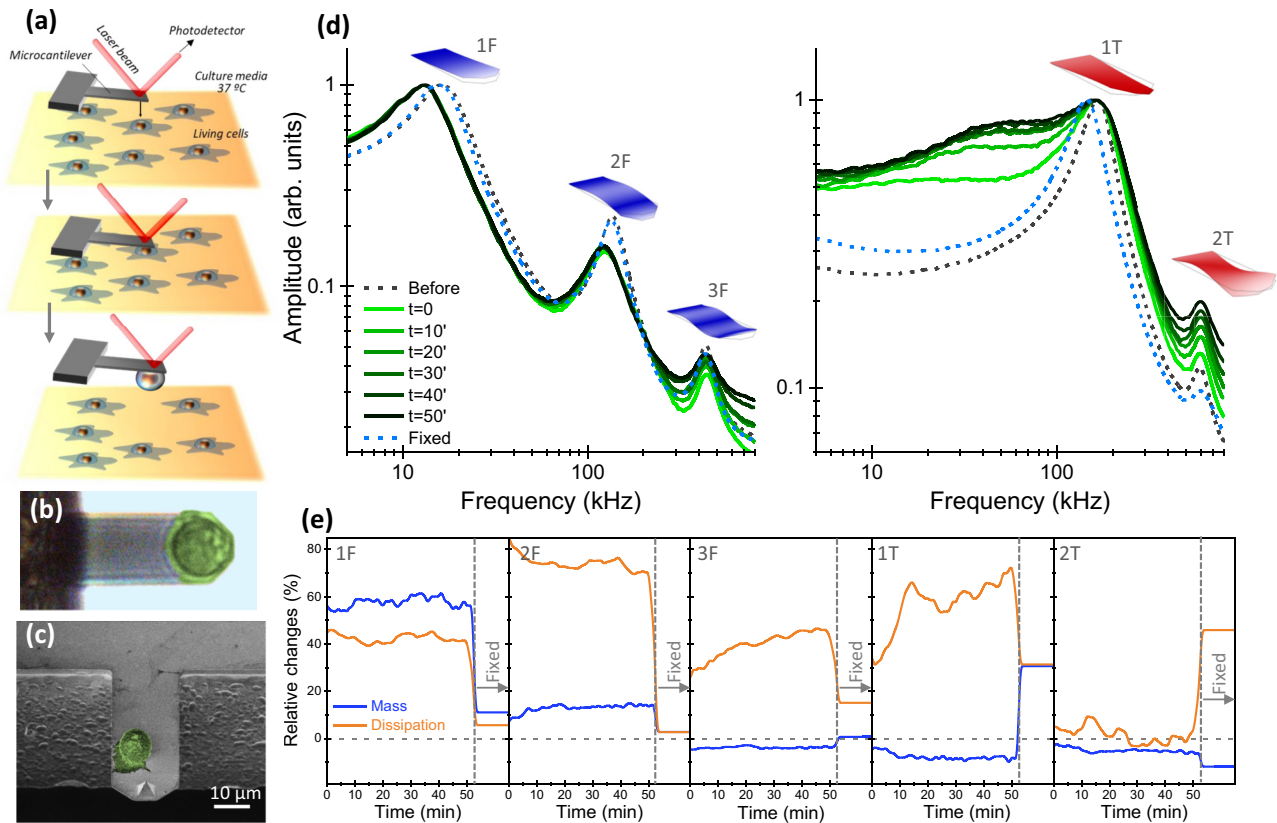
FIG. 3. Experimental realization and data analysis for unveiling mechanical resonances of living human cells in physiological conditions. (a) Schematic cartoon of the cell capture by the microcantilever. (b) Optical image of a MCF-10A breast epithelial cell adhered on the cantilever surface after its capture. (c) Scanning electron microscopy of a MCF-10A cell after fixation. (d) Frequency spectra of the thermal displacement fluctuations of the cantilever before the cell attachment, during cell attachment, and after cell fixation. The left and right graphs correspond to flexural-like and torsional-like oscillation that can be independently measured by the laser-beam deflection method. The frequency spectra of the unloaded cantilever show the first three flexural vibration modes labeled as 1F, 2F, and 3F, and the first two torsional vibration modes, as 1T and 2T. The mode shapes are included. (e) Fractional changes of the "apparent" mass added to the cantilever and energy dissipation of the system due to internal losses of the cell.

coupling [6,25] between the bending vibration mode of the cell and the first torsional mode of the cantilever. In order to confirm our theoretical assumptions, the cells were stiffened by using a fixative solution containing 8% paraformaldehyde and 8% glutaraldehyde for 15 min. Fixation produces covalent cross-linking between most of the molecules within the cell, resulting in a rigid and insoluble meshwork [26]. By using atomic force microscopy, we find that the MCF-10A cells stiffen by a factor between 8 and 20, which in turn induces an increase of the resonance frequency by a factor between 3 and 5. In addition, fixation can induce the reduction of the cell volume and loss of mass, contributing to a higher resonance frequency [27,28]. After replacing the fixative solution with the original growth media, the broad shoulder at the left side of the first torsional resonance peak disappears and the resonance frequency of the first torsional vibration mode of the cantilever downshifts –12% with respect to the unloaded cantilever. Interestingly, the resonance peak of the second torsional vibration mode becomes significantly broader. These observations indicate that fixation-induced stiffening of the cell shifts the bending resonance frequency of the cell to frequencies higher than that of the first torsional vibration mode of the cantilever.

The shape of the cantilever flexural spectra, on the other hand, is little modified upon cell attachment; however, the frequency and width of the three resonance peaks are notably changed. We analyze these changes by calculating the frequency and quality factors of the cantilever vibration modes by fitting the frequency spectra to a model that combines the damped harmonic oscillator model, the fluctuation-dissipation theorem [29,30], and fluid-cantilever interaction theory [31–33] (see Sec. III of the SM [17]). For the sake of convenience, we convert the resonance frequencies and quality factors (Q factors) into the following parameters [Fig. 3(a)] [34],

$$\mu_n = \left(\frac{\omega_{n,0}}{\omega_n}\right)^2 - 1, \qquad (4)$$

$$\zeta_n = \frac{Q_{n,0}}{Q_n} - \left(\frac{\omega_n}{\omega_{n,0}}\right)^2, \qquad (5)$$

where $\omega_{n,0}$ and ω_n are the resonance frequencies of the nth vibration mode of the cantilever, before and after attachment of the cell, and $Q_{n,0}$ and Q_n are the corresponding Q factors, before and after attachment of the cell. The first

parameter provides the relative increase of the cantilever apparent mass at the frequency of the nth vibration mode due to the cell attachment [34,35]. The second parameter [Eq. (5)] represents the relative change in system energy dissipation due to inherent losses within the cell (see Sec. I of the SM [17]).

This parameter is preferred over the change in quality factor because an increase in cantilever mass, resulting from a load without internal dissipation, alters the energy dissipation due to the change in viscous damping with frequency [32,36]. In such a scenario, the change in the Q factor is equivalent to the relative change in mass (μ_n), while ζ_n remains zero. More importantly, the proposed experimental observables are intimately connected to the vibrational properties of the cell through the following expressions,

$$\mu_n = \frac{m_c \langle \psi_n(x_0)^2 \rangle}{m_r} \mathrm{MTF}'(\omega_n), \qquad (6)$$

$$\zeta_n = \frac{m_c \langle \psi_n(x_0)^2 \rangle}{m_r} \left(\frac{\omega_n}{\omega_{n,0}} \right)^2 Q_{n,0} \mathrm{MTF}''(\omega_n), \qquad (7)$$

where m_c and m_r are the masses of the cell and the cantilever resonator in fluid, ψ_n is the normalized shape of the nth vibration mode of the cantilever, x_0 is the center position of the cell-cantilever contact, and $\langle \cdots \rangle$ stands for the average across the contact area. The relative increase of the resonator apparent mass μ_n and energy dissipation ζ_n follows a behavior similar to that of MTF$'$ and MTF$''$, respectively [Fig. 2(a)]. When $\omega_n \ll \omega_c$, the resonator operates in the mass sensor regime, with μ_n providing the ratio between the masses of the cell and the resonator times the amplitude mode shape and ζ_n being zero. In contrast, when $\omega_n \gg \omega_c$, both μ_n and ζ_n become zero, referred to as the "insensitive" sensing regime. The transition between these two regimes is broader when the cell dissipation is higher. In this transition regime, anomalies in the experimental observables may be expected, such as the decay of the apparent mass of the cell with frequency, the negative increase of apparent mass, or the maximum of ζ_n at frequencies near the cell resonance frequency.

We now turn our attention to the experimental data. After the cell attachment, the cantilever apparent mass increases at the frequencies of the first and second flexural vibration modes, but it decreases at the frequency of the third flexural vibration mode [Fig. 3(e)]. The apparent cell mass can be estimated by using the well-known equation in resonant mass sensors, $\Delta m_n = \frac{m_r \mu_n}{\langle \psi_n(x_0)^2 \rangle}$ [34,35]. Using this method for the first three flexural vibration modes, we obtain apparent cell masses of 4.08 ± 0.15 ng at 14 KHz, 1.5 ± 0.2 ng at 120 kHz, and -1.6 ± 0.3 ng at 430 kHz, respectively. The apparent cell mass decreases with frequency and becomes negative at higher frequencies, as was theoretically anticipated. Additionally, there is a significant increase in energy dissipation due to the cell at the resonance frequencies of the first three flexural vibration modes, with maximum dissipation at the second flexural mode. This suggests that the resonance frequency of the extensional vibration mode of the cell is near the frequency of the second flexural mode of the cantilever. Notably, the fractional change in energy dissipation is much higher than the relative change in apparent mass at the resonance frequencies of the second and third

flexural vibration modes. A negative apparent cell mass and very high dissipation are also observed for the cantilever's first torsional vibration mode. Following the fixation of the cell, there is a sudden decrease in energy dissipation across all vibration modes of the cantilever, with the exception of the second torsional vibration mode. In addition, the apparent added mass becomes positive in all vibration modes, again with the exception of the second torsional vibration mode. The smaller relative variations in mass observed in the flexural vibration modes of the cantilever can be attributed to a loss of cell mass during fixation [27,28] and the shift of the cell to a position further from the free end, where the amplitude of the eigenmodes is reduced. The increase of dissipation from near zero to 45% in the second torsional vibration mode is consistent with the shift of the bending resonance frequency of the cell from frequencies well below that of the second torsional vibration mode to near the resonance frequency of this mode.

The frequency spectra of the flexural and torsional fluctuations of the cantilever after the cell attachment are fitted to a stochastic coupling model grounded in our theory and the fluctuation-dissipation theorem, to determine the cell vibrational properties (see Sec. IV of the SM [17]). We assume that the high-frequency fluctuations under analysis are in equilibrium and are thermally driven. It is worth noting that active cell fluctuations resulting from ATP hydrolysis can also be coupled to the cantilever fluctuations, although this typically occurs at a much lower frequency range, 0.01–10 Hz [37,38]. In our model, the cantilever torsional oscillation triggers a transversal tilting motion in the cell, with minimal vertical displacement. In this scenario, the mass transfer function employed only accounts for the mechanical susceptibility of the cell bending vibration mode [Eq. (1)]. Flexural oscillation of the cantilever involves two types of motion: vertical displacement and longitudinal tilting motion. The latter is negligible for the first flexural vibration mode near the free end of the cantilever where the cell adheres. However, for the second and third flexural vibration modes, which display the primary anomalies upon cell attachment, the longitudinal tilting and vertical displacement are comparable (see Sec. V of the SM [17]). To acquire precise data on the cell extensional vibration mode, we fit the region of the flexural vibration spectra encompassing the second and third vibration modes of the cell. We use a mass transfer function that includes the responses of both the cell fundamental bending vibration mode (previously obtained from fitting the torsional frequency spectra) and the cell first extensional vibration mode. The obtained mass transfer functions are shown in Fig. 4(a) and the resonance frequencies and power-law exponents of the cell vibration modes are shown in Fig. 4(b). The frequency of the fundamental bending vibration mode of the cell rapidly increases from 10 to 28 kHz in the first 14 min, then slowly rises to 34 kHz over the remaining 28 min of the experiment. The power-law exponent remains relatively stable, ranging from 0.72 to 0.77. The MTF obtained for the cantilever flexural spectra shows initial localization of cell fluctuations in the bending vibration mode, but the contribution of the extensional vibration mode increases over time. The resonance frequency of the first extensional vibration mode rises from 155 to 190 kHz. The power-law exponent, in turn, increases
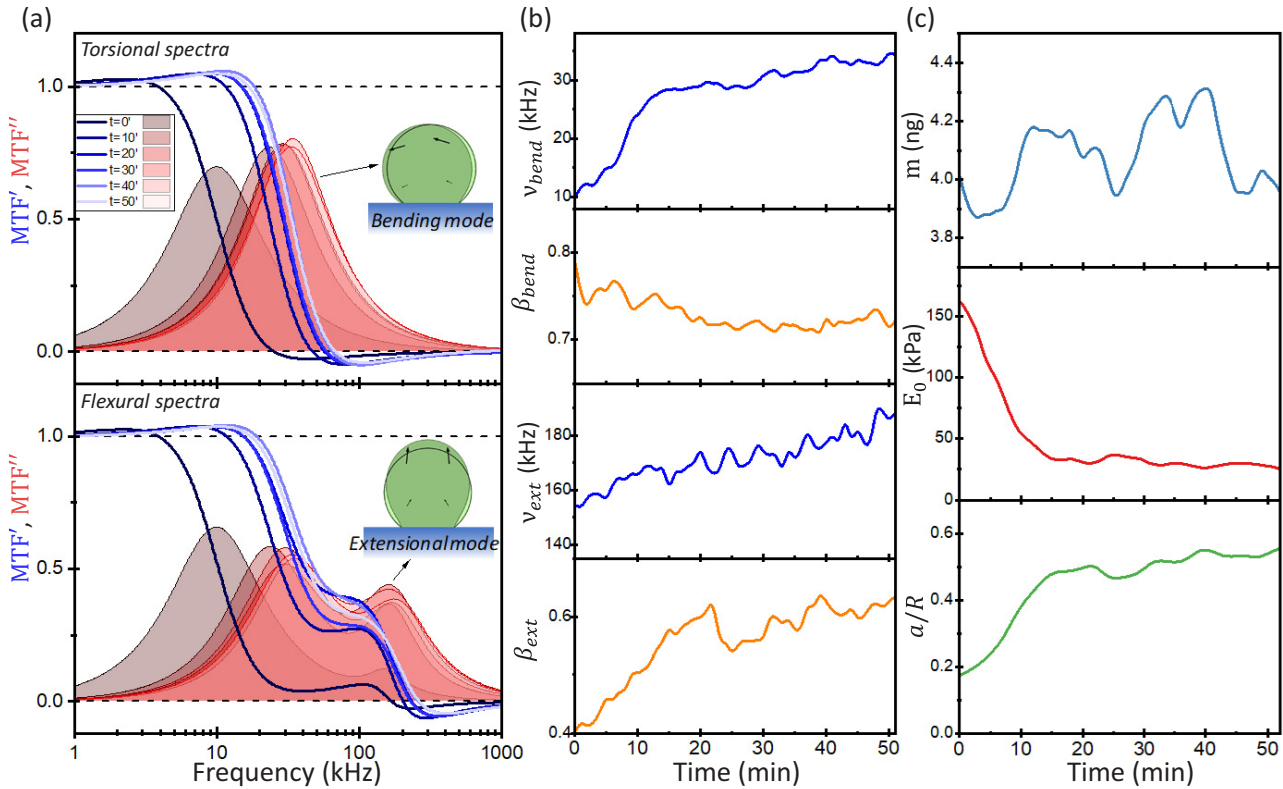
FIG. 4. Retrieving the vibrational properties of living cells adhered to a cantilever by fitting the stochastic frequency response of the cantilever to our theoretical model. (a) Real and (minus) imaginary parts of the mass transfer function obtained from frequency spectra of the torsional (top) and flexural (bottom) fluctuations of the cantilever with the MCF-10A cell shown in Fig. 3. The MTF for the torsional fluctuations is primarily determined by the cell's fundamental bending vibration mode. In contrast, for flexural fluctuations, both the bending and first extensional vibration modes contribute to the MTF. (b) Resonance frequency ($\upsilon = \frac{\omega}{2\pi}$) and power-law exponent (β) of the fundamental bending (*bend*) and first extensional (*ext*) vibration modes. (c) Theoretical estimation of the cell's mass, elasticity modulus at 10 kHz, and contact radius to cell radius ratio.

from 0.4 to 0.6 during the first 20 min, and then it grows at a much slower rate.

Close examination of the theoretical and experimental data reveals information about the cell physical properties and the adhesion process [39] [Fig. 4(c)]. We find that the effect of the cell vibration modes on the resonance frequency of the first flexural vibration mode of the cantilever is marginal ($<3\%$) (see Sec. V of the SM [17]). Therefore, this mode operates in the mass sensor regime enabling the determination of the cell mass [22,23,40,41]. Compared to the cell's vibrational properties, the mass remains relatively stable oscillating by about 5% at irregular periods of about 10 min. On the other hand, the resonance frequencies of the bending and extensional modes of the cell follow a different dependence on the contact area [Eq. (3)]. The fundamental bending vibration mode is highly sensitive to the contact area. For small contact areas $\lambda_{\text{bend}} \sim (\frac{a}{R})^{1.4}$, whereas for the first extensional vibration mode $\lambda_{\text{ext}} \sim (\frac{a}{R})^{0.6}$. This difference is used to estimate the contact area and the elasticity modulus at a reference frequency of 10 kHz [Fig. 4(c)]. The resulting data show that the cell initially adheres with a small contact area ($a/R \approx 0.2$), and it rapidly strengthens its anchorage during the first 14 min, reaching $a/R \approx 0.5$. This is followed by a slower adhesion process during the rest of the experiment, reaching $a/R \approx$

0.55. In parallel, the elasticity modulus decreases rapidly from 160 to 35 kPa in the first 14 min, then slowly decreases to 25 kPa by the end of the experiment. These values are consistent with previous reports [12,21]. The initial drop in cell stiffness has been linked to a temporary decrease in cortical and membrane tension required for spreading [42]. The observations detailed in this study have also been identified in other MCF-10A cells, as well as in low invasive breast cancer MCF-7 cells and metastatic breast cancer MDA-MB-231 cells. This underscores the universal nature of these findings across complex eukaryotic cells, such as human cells, under physiological conditions (see Sec. VI of the SM [17]).

In conclusion, we have demonstrated that complex living cells in physiological conditions do exhibit detectable vibration modes, addressing a question posed by Ackerman during the 1950s [1,3]. Our method has potential for cell fingerprinting, but improvements are needed due to the low quality factor of the cell bending vibration mode and the weaker effect of the extensional vibration mode. We foresee enhancements through the design of micromechanical resonators operating at higher frequencies [43], enabling observation of more cell vibration modes with higher resolution. The use of excitation methods could also improve the signal-to-noise ratio and exploit cell deformation nonlinearities to increase sensitivity

[19,44]. These advances could lead to new approaches for vibration spectrometry of living cells and potentially revive the idea of destroying cancerous cells by targeting specific cell frequencies with focused ultrasonic waves [13]. Emerging research is beginning to unveil the effect of mechanical vibrations in the low-frequency range, 1–100 Hz, on the cellular behavior [14–16]. The precise mechanisms through which these vibrations exert their effects are still being explored, but the findings to date suggest a complex interplay between mechanical forces and cellular biology. Our findings open up avenues for future research into the impact of mechanical resonances on cell survival, proliferation, and migration, which are critical aspects of cellular biology and cancer disease.

IV. METHODS

Cell culture. The MCF-10A cell line was purchased from the American Type Culture Collection (ATCC, USA). MCF-10A were grown in DMEM/F12 medium (Gibco, Life Technologies Corporation, USA) supplemented with 5% horse serum, 20 ng/ml epidermal growth factor, 0.5 µg/ml hydrocortisone, 100 ng/ml cholera toxin, 10 µg/ml insulin, 500 U/ml penicillin, and 0.1 mg/ml streptomycin.

Cantilever beam and functionalization. We used silicon nitride cantilevers with nominal length of 50 µm, width of 20 µm, and thickness of 0.21 µm (SD-nAmbition Array5, Nanoworld, Switzerland). Both cantilever sides are coated with 2–3 nm of Cr and 30 nm of Au. The nominal spring constant was 0.17 N/m. Prior to cantilever functionalization, cantilever arrays were cleaned with piranha solution (2 H_2SO_4:1 H_2O_2) for 15 min at room temperature (RT) (*caution: piranha solution is extremely corrosive, reactive, and potentially explosive*) to remove all the organic residues on the surface. Then, the cantilevers were extensively rinsed with Milli-Q water and dried under a stream of nitrogen (N_2). After that the cantilevers were incubated with a 100 µg/ml solution of thiol PEG amine (HS-PEG2K-NH_2, M_n 2000, Sigma Aldrich) in degassed Milli-Q water for 1 h at 25 °C under agitation. The samples were then rinsed with Milli-Q water and dried with N_2. Next, the cantilevers were immersed in a 2 mg/ml solution of 4-(*N*-maleimidomethyl) cyclohexane-1-carboxylic acid 3-sulfo-*N*-hydroxysuccinimide ester sodium salt (Sulfo-SMCC, Sigma Aldrich) in phosphate-buffered saline (PBS) (*p*H7.4) for 2 h, at RT in N_2 atmosphere, and protected from light. The cantilevers were subsequently washed twice with PBS, rinsed with Milli-Q water, and dried under a stream of N_2. Afterwards, the cantilevers were dipped into a 20 µg/ml of fibronectin (Sigma Aldrich) in PBS (*p*H7.4) and incubated for 3 h at 25 °C under agitation. The cantilevers were stored at 4 °C until its use, which was no longer than 4 days. Finally, the cantilevers were washed with PBS, Milli-Q water, and dried with N_2.

Measurements. The cantilever thermal fluctuations were measured using a JPK NanoWizard 4 AFM (Bruker) mounted on an inverted microscope (Leica DMI6000-CS, Germany). The AFM photodetector signals were processed using custom software developed in LABVIEW (National Instruments, Austin, USA). Optical images of the cantilever and cells were captured using a 40× objective (Leica, HC PL Fluotar L 40×/0.60, Spain). Cells were maintained in physiological conditions during measurements using a heater that kept cell cultures at 37 °C. Cells were seeded at a density of 4×10^4 cells/ml onto untreated lids of 35 mm cell culture plates (Corning CellBIND Surface) with 3 ml of their respective medium for 24 h before the experiment. Untreated lids were used to facilitate cell detachment from the culture plate and subsequent attachment to the fibronectin-functionalized cantilever surface. Cell attachment was achieved by positioning the cantilever free end above the center of a selected cell and applying a force of 3 nN during 10 min. Afterward, the cantilever with the attached cell was retracted 200 µm. The frequency spectra of the displacement fluctuations of the cantilever were recorded before and after the cell attachment for approximately 1 h (one measurement every 60 s). After that, the cell was fixed by adding 1 ml of 4× fixing medium [8% paraformaldehyde + 8% glutaraldehyde, in phosphate buffer (*p*H7.4)] to the culture media, to achieve a fixative solution concentration of 1×. After incubating for 15 min at RT, the solution was replaced by the culture media. Custom software written in *Wolfram Mathematica* was used to process and analyze the optical images and recorded frequency spectra.

FEM simulations. FEM simulations were carried using the commercial software COMSOL MULTIPHYSICS. Eigenfrequency and frequency domain studies were carried out within the SOLID MECHANICS and the THERMOVISCOUS ACOUSTICS module for the surrounding fluid.

[1] E. Ackerman, Mechanical resonances of amphiuma erythrocytes, J. Acoust. Soc. Am. **26**, 257 (1954).

[2] H. Kinsloe, E. Ackerman, and J. J. Reid, Exposure of microorganisms to measured sound fields, J. Bacteriol. **68**, 373 (1954).

[3] E. Ackerman, Resonances of biological cells at audible frequencies, Bull. Math. Biophys. **13**, 93 (1951).

[4] P. V. Zinin, J. S. Allen, and V. M. Levin, Mechanical resonances of bacteria cells, Phys. Rev. E **72**, 061907 (2005).

[5] P. V. Zinin and J. S. Allen, Deformation of biological cells in the acoustic field of an oscillating bubble, Phys. Rev. E **79**, 021910 (2009).

[6] E. Gil-Santos, J. J. Ruz, O. Malvar, I. Favero, A. Lemaître, P. M. Kosaka, S. García-López, M. Calleja, and J. Tamayo, Optomechanical detection of vibration modes of a single bacterium, Nat. Nanotechnol. **15**, 469 (2020).

[7] S.-J. Tang, M. Zhang, J. Sun, J.-W. Meng, X. Xiong, Q. Gong, D. Jin, Q.-F. Yang, and Y.-F. Xiao, Single-particle photoacoustic vibrational spectroscopy using optical microresonators, Nat. Photon. **17**, 951 (2023).

[8] E. Moeendarbary, L. Valon, M. Fritzsche, A. R. Harris, D. A. Moulding, A. J. Thrasher, E. Stride, L. Mahadevan, and G. T. Charras, The cytoplasm of living cells behaves as a poroelastic material, Nat. Mater. **12**, 253 (2013).

[9] J. Hu, S. Jafari, Y. Han, A. J. Grodzinsky, S. Cai, and M. Guo, Size- and speed-dependent mechanical behavior in living mammalian cytoplasm, Proc. Natl. Acad. Sci. USA **114**, 9529 (2017).

[10] M. L. Yubero, P. M. Kosaka, Á. San Paulo, M. Malumbres, M. Calleja, and J. Tamayo, Effects of energy metabolism on the mechanical properties of breast cancer cells, Commun. Biol. **3**, 590 (2020).

[11] Y. M. Efremov, A. X. Cartagena-Rivera, A. I. M. Athamneh, D. M. Suter, and A. Raman, Mapping heterogeneity of cellular mechanics by multi-harmonic atomic force microscopy, Nat. Protoc. **13**, 2200 (2018).

[12] A. Rigato, A. Miyagi, S. Scheuring, and F. Rico, High-frequency microrheology reveals cytoskeleton dynamics in living cells, Nat. Phys. **13**, 771 (2017).

[13] A. Geltmeier, B. Rinner, D. Bade, K. Meditz, R. Witt, U. Bicker, C. Bludszuweit-Philipp, and P. Maier, Characterization of dynamic behaviour of MCF7 and MCF10A cells in ultrasonic field using modal and harmonic analyses, PLoS ONE **10**, e0134999 (2015).

[14] P. G. Childs, C. A. Boyle, G. D. Pemberton, H. Nikukar, A. S. G. Curtis, F. L. Henriquez, M. J. Dalby, and S. Reid, Use of nanoscale mechanical stimulation for control and manipulation of cell behaviour, Acta Biomater. **34**, 159 (2016).

[15] G. Bas, S. Loisate, S. F. Hudon, K. Woods, E. J. Hayden, X. Pu, R. Beard, J. T. Oxford, and G. Uzer, Low intensity vibrations augment mesenchymal stem cell proliferation and differentiation capacity during *in vitro* expansion, Sci. Rep. **10**, 9369 (2020).

[16] A. Tijore, M. Yao, Y.-H. Wang, A. Hariharan, Y. Nematbakhsh, B. L. Doss, C. T. Lim, and M. Sheetz, Selective killing of transformed cells by mechanical stretch, Biomaterials **275**, 120866 (2021).

[17] See Supplemental Material at http://link.aps.org/supplemental/10.1103/PRXLife.2.013003 for additional information.

[18] A. F. Bower, *Applied Mechanics of Solids* (CRC Press, Boca Raton, FL, 2009).

[19] P. Kollmannsberger and B. Fabry, Linear and nonlinear rheology of living cells, Annu. Rev. Mater. Res. **41**, 75 (2011).

[20] Y. M. Efremov, W.-H. Wang, S. D. Hardy, R. L. Geahlen, and A. Raman, Measuring nanoscale viscoelastic parameters of cells directly from AFM force-displacement curves, Sci. Rep. **7**, 1541 (2017).

[21] G. Fläschner, C. I. Roman, N. Strohmeyer, D. Martinez-Martin, and D. J. Müller, Rheology of rounded mammalian cells over continuous high-frequencies, Nat. Commun. **12**, 2922 (2021).

[22] D. Martínez-Martín, G. Fläschner, B. Gaub, S. Martin, R. Newton, C. Beerli, J. Mercer, C. Gerber, and D. J. Müller, Inertial picobalance reveals fast mass fluctuations in mammalian cells, Nature (London) **550**, 500 (2017).

[23] I. Incaviglia, S. Herzog, G. Fläschner, N. Strohmeyer, E. Tosoratti, and D. J. Müller, Tailoring the sensitivity of microcantilevers to monitor the mass of single adherent living cells, Nano Lett. **23**, 588 (2023).

[24] J. Tamayo, J. J. Ruz, V. Pini, P. Kosaka, and M. Calleja, Quantification of the surface stress in microcantilever biosensors: Revisiting Stoney's equation, Nanotechnology **23**, 475702 (2012).

[25] E. Gil-Santos, D. Ramos, A. Jana, M. Calleja, A. Raman, and J. Tamayo, Mass sensing based on deterministic and stochastic responses of elastically coupled nanocantilevers, Nano Lett. **9**, 4122 (2009).

[26] S.-O. Kim, J. Kim, T. Okajima, and N.-J. Cho, Mechanical properties of paraformaldehyde-treated individual cells investigated by atomic force microscopy and scanning ion conductance microscopy, Nano Convergence **4**, 5 (2017).

[27] J. W. Choi and D. K. Stoecker, Effects of fixation on cell volume of marine planktonic protozoa, Appl. Environ. Microbiol. **55**, 1761 (1989).

[28] R. Cheng, F. Zhang, M. Li, X. Wo, Y.-W. Su, and W. Wang, Influence of fixation and permeabilization on the mass density of single cells: A surface plasmon resonance imaging study, Front. Chem. **7**, 588 (2019).

[29] P. R. Saulson, Thermal noise in mechanical experiments, Phys. Rev. D **42**, 2437 (1990).

[30] M. R. Paul, M. T. Clark, and M. C. Cross, The stochastic dynamics of micron and nanoscale elastic cantilevers in fluid: Fluctuations from dissipation, Nanotechnology **17**, 4502 (2006).

[31] C. A. Van Eysden and J. E. Sader, Frequency response of cantilever beams immersed in viscous fluids with applications to the atomic force microscope: Arbitrary mode order, J. Appl. Phys. **101**, 044908 (2007).

[32] S. Basak, A. Raman, and S. V. Garimella, Hydrodynamic loading of microcantilevers vibrating in viscous fluids, J. Appl. Phys. **99**, 114906 (2006).

[33] J. E. Sader, J. A. Sanelli, B. D. Adamson, J. P. Monty, X. Wei, S. A. Crawford, J. R. Friend, I. Marusic, P. Mulvaney, and E. J. Bieske, Spring constant calibration of atomic force microscope cantilevers of arbitrary shape, Rev. Sci. Instrum. **83**, 103705 (2012).

[34] J. Tamayo, P. M. Kosaka, J. J. Ruz, Á. S. Paulo, and M. Calleja, Biosensors based on nanomechanical systems, Chem. Soc. Rev. **42**, 1287 (2013).

[35] A. Sanz-Jiménez *et al.*, High-throughput determination of dry mass of single bacterial cells by ultrathin membrane resonators, Commun. Biol. **5**, 1227 (2022).

[36] R. R. Grüter *et al.*, Disentangling mechanical and mass effects on nanomechanical resonators, Appl. Phys. Lett. **96**, 023113 (2010).

[37] M. Guo, A. J. Ehrlicher, M. H. Jensen, M. Renz, J. R. Moore, R. D. Goldman, J. Lippincott-Schwartz, F. C. Mackintosh, and D. A. Weitz, Probing the stochastic, motor-driven properties of the cytoplasm using force spectrum microscopy, Cell **158**, 822 (2014).

[38] G. Longo, L. Alonso-Sarduy, L. M. Rio, A. Bizzini, A. Trampuz, J. Notz, G. Dietler, and S. Kasas, Rapid detection of bacterial resistance to antibiotics using AFM cantilevers as nanomechanical sensors, Nat. Nanotechnol. **8**, 522 (2013).

[39] D. Cuvelier, M. Théry, Y.-S. Chu, S. Dufour, J.-P. Thiéry, M. Bornens, P. Nassoy, and L. Mahadevan, The universal dynamics of cell spreading, Curr. Biol. **17**, 694 (2007).

[40] A. P. Cuny, K. Tanuj Sapra, D. Martinez-Martin, G. Fläschner, J. D. Adams, S. Martin, C. Gerber, F. Rudolf, and D. J. Müller, High-resolution mass measurements of single budding yeast reveal linear growth segments, Nat. Commun. **13**, 3483 (2022).

[41] E. A. Corbin, O. O. Adeniba, O. V. Cangellaris, W. P. King, and R. Bashir, Evidence of differential mass change rates between human breast cancer cell lines in culture, Biomed. Microdevices **19**, 10 (2017).

[42] A. Pietuch and A. Janshoff, Mechanics of spreading cells probed by atomic force microscopy, Open Biol. **3**, 130084 (2013).

[43] H. Kähler, H. Arthaber, R. Winkler, R. G. West, I. Ignat, H. Plank, and S. Schmid, Transduction of single nanomechanical pillar resonators by scattering of surface acoustic waves, Nano Lett. **23**, 4344 (2023).

[44] S. Tiwari and R. N. Candler, Using flexural MEMS to study and exploit nonlinearities: A review, J. Micromech. Microeng. **29**, 083002 (2019).